Clinical Immunology 208 (2019) 108232

Contents lists available at ScienceDirect

Clinical Immunology

journal homepage: www.elsevier.com/locate/yclim

CASP1 variants influence subcellular caspase-1 localization, pyroptosome formation, pro-inflammatory cell death and macrophage deformability

Franz Kapplusch[a,d,1], Felix Schulze[a,1], Sabrina Rabe-Matschewsky[a], Susanne Russ[a], Maik Herbig[b], Michael Christian Heymann[a], Katharina Schoepf[a], Robert Stein[a], Ursula Range[c], Angela Rösen-Wolff[a], Stefan Winkler[a], Christian Michael Hedrich[a,d,e], Jochen Guck[b], Sigrun Ruth Hofmann[a,*]

[a] Department of Pediatrics, Medizinische Fakultät Carl Gustav Carus, Technische Universität Dresden, Dresden, Germany
[b] Biotechnology Center for Molecular and Cellular Bioengineering, Technische Universität Dresden, Dresden, Germany
[c] Institute for Medical Informatics and Biometry, Medizinische Fakultät Carl Gustav Carus, Technische Universität Dresden, Dresden, Germany
[d] Department of Women's & Children's Health, Institute of Translational Medicine, University of Liverpool, Liverpool, UK
[e] Department of Paediatric Rheumatology, Alder Hey Children's NHS Foundation Trust Hospital, Liverpool, UK

ARTICLE INFO

Keywords:
Caspase-1
Inflammasome
NLRP3
IL-1β
Interleukin-1 converting enzyme
Apoptosis-associated speck-like protein containing a CARD (ASC)
Pyroptosome
Pyroptosis
Speck
Gasdermin D

ABSTRACT

CASP1 variants result in reduced enzymatic activity of procaspase-1 and impaired IL-1β release. Despite this, affected individuals can develop systemic autoinflammatory disease. These seemingly contradictory observations have only partially been explained by increased NF-κB activation through prolonged interaction of variant procaspase-1 with RIP2. To identify further disease underlying pathomechanisms, we established an *in vitro* model using shRNA-directed knock-down of procaspase-1 followed by viral transduction of human monocytes (THP-1) with plasmids encoding for wild-type procaspase-1, disease-associated *CASP1* variants (p.L265S, p.R240Q) or a missense mutation in the active center of procaspase-1 (p.C285A). THP1-derived macrophages carrying *CASP1* variants exhibited mutation-specific molecular alterations. We here provide *in vitro* evidence for abnormal pyroptosome formation (p.C285A, p.240Q, p.L265S), impaired nuclear (pro)caspase-1 localization (p.L265S), reduced pro-inflammatory cell death (p.C285A) and changes in macrophage deformability that may contribute to disease pathophysiology of patients with *CASP1* variants. This offers previously unknown molecular pathomechanisms in patients with systemic autoinflammatory disease.

1. Introduction

Naturally occurring variants of the caspase-1 (*CASP1*) gene were identified in patients with recurrent fevers and other signs of systemic inflammation.1 The term *CASP1*-associated autoinflammatory disease (CASP1-AID) has been suggested for this disorder. In most cases, symptoms start in early childhood and include febrile episodes (> 38.5 °C) lasting 3 days to 3 weeks, systemic inflammation with C-reactive protein elevation > 50 mg/l, and additional complaints, including arthralgia, myalgia and/or exanthema. Some patients exhibit abdominal pain, diarrhea, and lymphadenopathy.

The *CASP1* gene locates to chromosome 11q22.3, comprises 10 exons (NM_033292; NCBI RefSEq.2) and encodes for procaspase-1. Most of the identified point mutations are located in exon 6, which encodes for the p20 subunit of procaspase-1. Thus, mutations closely localize to the active center of caspase-1 and interfere with hetero-tetramer formation through destabilization of water-mediated hydrogen bonds and hydrophobic interactions at the dimer-dimer interface.1

Caspase-1 is activated in response to the recognition of pathogen and/or danger associated molecular patterns (PAMPs or DAMPs) through intracellular sensors including NOD-like receptors (NLR). This results in a conformational change allowing for associations with the apoptosis associated speck-like protein containing a CARD (ASC), leading to caspase-1 activation and enzymatic cleavage of pro-interleukin (IL)-1β and pro-IL-18 into their active forms. Furthermore, direct proximity of procaspase-1 molecules results in auto-processing and activation of caspase-1 into the N-terminal caspase recruitment domain (CARD), a central p20 and a C-terminal p10 subunit. The hetero-tetrameric assembly of two p10 and two p20 subunits results in active caspase-1.

* Correspondence author at: Department of Pediatrics, University Hospital Carl Gustav Carus, Fetscherstrasse 74, 01307 Dresden, Germany.
E-mail address: sigrun.hofmann@uniklinikum-dresden.de (S.R. Hofmann).
[1] contributed equally

https://doi.org/10.1016/j.clim.2019.06.008
Received 7 April 2019; Received in revised form 27 May 2019; Accepted 24 June 2019
Available online 26 June 2019
1521-6616/

The analysis of caspase-1 variants in an *in vitro* cell model (resembling the cellular phenotype of CASP1-AID) revealed variant-specific decreased or abrogated enzymatic activity of caspase-1 and subsequently impaired IL-1β secretion.[1] Whole blood samples of patients confirmed reduced IL-1β secretion, however, elevated expression of pro-inflammatory TNF-α.[1] The paradox of an inflammatory phenotype in the absence of caspase-1 enzyme activity led to the hypothesis of up-regulated alternative pro-inflammatory pathways in individuals with *CASP1* variants. Recently, we supported this hypothesis by demonstrating enhanced NF-κB activation through variant procaspase-1, which is dependent on receptor interacting protein kinase (RIP)2. In the context of CASP1-AID, CARD:CARD interactions between RIP2 and procaspase-1 variants are stabilized which results in increased NF-κB activation.[3]

Caspase-1 is not only a key regulator of the innate immune response activating pro-inflammatory cytokines IL-1β and IL-18. It also promotes pyroptosis, an inflammatory form of programmed cell death, by cleaving the pore-forming effector protein gasdermin D (GSDMD).[4] This leads to plasma membrane pore formation, cell swelling and burst by osmotic lysis and subsequently the release of highly pro-inflammatory cellular components.[5,6] Pyroptosis is further characterized by the formation of a macromolecular ASC aggregate (ASC speck) preceding cell swelling and cell death. ASC speck formation has first been described in 1999 in promyelocytic leukemia HL-60 cells, where it was linked to apoptosis.[7] Fernandes-Alnemri et al. extended this notion by observing cytosolic ASC speck formation in the perinuclear region of immune cells (monocytes) after lipopolysaccharide (LPS) stimulation, subsequently inducing pyroptosis.[8] Therefore, authors introduced the term “pyroptosome” for this spherical cytosolic ASC-aggregate/-speck. Recently, “pyroptosome” polymerization mechanisms have been revealed up to an almost molecular level.[9,10] After recognition of PAMPs or DAMPs by pyrin domain (PYD) containing receptors, such as NLRP3 or AIM2, these receptors oligomerize and attract the adapter protein ASC through heterotypic PYD:PYD interaction. The PYD of ASC forms helical filamentous structures (*via* homotypic PYD:PYD interaction), exposing the CARD of ASC in the periphery. CARD domains further recruit procaspase-1 through heterotypic CARD:CARD interaction[9,10] forming a macromolecular speck complex. Though still subject of ongoing discussions, the formation of pyroptosomes and inflammasomes are currently considered to be the same phenomenon.[11] Taken together, ASC specks serve as activation platforms, recruiting and activating caspase-1. Of note, speck formation is required for IL-1β processing but not for induction of cell death.[12] Recently, it has been described that pyroptosomes/specks released after cell lysis remained active in the extracellular compartment and kept processing procaspase-1 and pro-IL-1β.[13,14] Furthermore, specks were engulfed by macrophages, hence amplifying inflammatory responses in receiving cells. The *in vivo* relevance of pyroptosome uptake has been highlighted by detecting increased levels of pyroptosomes in sera from patients with cryopyrin associated periodic syndrome (CAPS), an autoinflammatory disease with gain-of-function mutations within the NLRP3 gene.[13]

Additionally, ASC was suggested to compete with the CARD domain of RIP2 for binding to the procaspase-1 CARD domain, thereby leading to the down-regulation of RIP2-mediated NF-κB activation.[15] Furthermore, ASC is reported to modulate actin polymerization, thus influencing migration of lymphocytes.[16] Finally, ASC activates the transcription of a variety of regulators of apoptosis, cell proliferation and differentiation, including the initiator caspases −8 and − 9, the effector caspase-3, AP-1 signaling pathways (among others inducing the pro-inflammatory chemokine IL-8), mitogen-activated protein kinases (MAPK) and NF-κB.[17–21]

This study was to investigate molecular alterations caused by *loss-of-function* mutations in the *CASP1* gene of patients with CASP1-AID. We provide *in vitro* evidence of the importance of pyroptosome formation and macrophage deformability in the molecular pathophysiology of CASP1-AID.

2. Materials and methods

2.1. Plasmids

The plasmid encoding human procaspase-1 was a kind gift from Prof. J. Tschopp (University of Lausanne, Lausanne, Switzerland). The procaspase-1 p.R240Q, p.L265S and p.C285A variants were generated by site directed mutagenesis using the QuickChangeII XL Site-Directed Mutagenesis Kit (Stratagene, La Jolla, CA) following standard protocols. cDNA fragments of wild type procaspase-1 and the variants were cloned into the lentiviral transfer vector p6NST51 or p6NST53 (kindly provided by Prof. Dirk Lindemann, Institute of Virology, University Hospital Carl Gustav Carus, Technische Universität Dresden, Germany) and fused to either mCherry or pEGFP at their N-terminus. The two plasmids p6NST51 and p6NST53 only differed in their resistance for eukaryotic selection and are a variant of p6NST50.[22,23] mCherry and EGFP plasmids were purchased from Clontech (Mountain View, CA). All constructs underwent quality control by restriction enzyme digestion and Sanger sequencing.

2.2. Antibodies and reagents

The following antibodies were used: anti-IL-1β (H-153, sc-7884), anti-procaspase-1 (A-19; sc-622), anti-caspase-1 p20 (C-15; sc-1780), anti-caspase-1 p10 (M-20; sc-514), anti-GSDMD (H-6, sc-376318) (all Santa Cruz Biotechnology, Santa Cruz, CA); anti-ASC (AL177; AdipoGen, Epalinges, Schweiz), anti-mCherry (1C51; Abcam, Cambridge, UK), anti-β-Actin (A2228; Sigma-Aldrich, St. Louis, USA), horseradish peroxidase (HRP)-linked anti-rabbit (NA9340; GE Healthcare, Freiburg, Germany), HRP-linked anti-mouse (P0260; DakoCytomation, Glostrup, Denmark), HRP-linked anti-goat (AP186P; Merck Millipore, Billerica, USA), Alexa Fluor 488-linked anti-rabbit (A-11008), Alexa Fluor 488-linked anti-mouse (A-11001) (both Life Technologies, Darmstadt, Germany).

Nigericin and ultra-pure LPS (uLPS) from *E. coli* O111:B4 were obtained from InvivoGen (Toulouse, France). Nuclei in life cell imaging experiments were stained with NucBlue® Live ReadyProbes® Reagent (ThermoFisher Scientific, Schwerte, Germany).

2.3. Cell lines and cell culture procedures

We established an *in vitro* model of a virally transduced human monocytic cell line (THP-1, ATCC TIB-202, LGC Standards GmbH, Wesel, Germany) with shRNA knock-down of endogenous procaspase-1 (a-PCasp1, against the 3’-UTR) reconstituted with either wildtype or variant procaspase-1 fusion-reporter proteins. Briefly, the expression of endogenous procaspase-1 was knocked down using the shRNA expression vector plKO.1 (Addgene, Cambridge, MA). The following target sequences were used: *CASP1*–3′-untranslated region, AAGAGATCCTT CTGTAAAGGT and control, AAGACCTCTTGTTAAGAGAGT. Lentiviral vector particles were produced in HEK293T cells (ATCC, LGC Standards GmbH, Wesel, Germany) transfected with lentiviral expression plasmid and plasmids psPAX2 and pVSVg. THP-1 cells were transduced with plkO.1 lentiviral stocks and selected with puromycin. Protein knock-down was analyzed by Western blotting. This cell line was then reconstituted with wildtype or variant caspase-1 by transduction of lentiviral vector particles, produced as described above, with a multiplicity of infection (MOI) of 0.1 (p6NST51.mCherry.CASP1) or 0.2 (p6NST53.EGFP.CASP1) and selected with zeocin or G418 respectively. THP-1 cells were cultivated in 5% CO_2 at 37 °C in RPMI medium 1640 supplemented with 2 mM L-glutamine, 10% fetal calf serum (FCS) and 100 U/ml penicillin and 100 µg/ml streptomycin (all Life Technologies).

HEK 293 T cell lines were grown at 37 °C in humidified atmosphere of air with 5% CO2 in DMEM supplemented with 2 mM L-glutamine, 10% FCS and penicillin/ streptomycin.

2.4. Image processing and quantification of pyroptosome formation

Pyroptosome formation in THP-1 cells was analyzed by immunofluorescence analysis of mCherry/EGFP caspase-1 specks. THP-1 cells were seeded in 0.7 cm^2 chambers (8-well Lab-Tek chambered coverglass system; ThermoFisher Scientific), stimulated as described, stained with NucBlue® Live ReadyProbes® Reagent (ThermoFisher Scientific, Schwerte, Germany) and subsequently imaged using a Zeiss Axiovert 200 M microscope (Carl Zeiss Microscopy GmbH, Germany) and a Zeiss Plan-Apochromat 10×/0.45NA objective and reflectors for Hoechst staining (EX 340–380 nm, EM 435–485 nm), GFP (EX 465–495 nm, EM 500-540 nm) and cherry (EX 530–560 nm, EM 590–650 nm). A CCD Coolsnap HQ camera (Photometrics, USA) and Visiview/MetaMorph (Visitron Systems GmbH, Puchheim, Germany) software was used for data acquisition. Live cell imaging was conducted in RPMI (ThermoFisher Scientific) at 37 °C and 5% CO_2 at the light microscopy facility BIOTEC/CRTD.

Image processing was carried out with ImageJ/Fiji software24(http://imagej.nih.gov/ij/; http://fiji.sc/Fiji). Specks/pyroptosomes were counted manually in the mCherry- or GFP-channel, total cell numbers were determined by quantification of nuclei in the Hoechst channel. Speck intensity was measured as the maximum intensity of each speck. For analysis of the speck diameter, the full-width at half-maximum intensity was applied.

2.5. Protein expression analysis

Caspase-1 was measured in serum-free cell supernatants or cell lysates by SDS PAGE, using anti-caspase-1 (M-20, sc-514), and anti-IL-1β (H-153, sc-7884) (both Santa Cruz, CA). Cells were lysed and processed as reported previously.3,15

2.6. Measurement of secreted IL-1β

Concentrations of mature IL-1β in the supernatant were determined using *cytometric bead arrays* (CBA) from Becton Dickinson (Franklin Lakes, NJ).

Immunoblotting of precipitated supernatant was performed by adding an equal volume of methanol and 0.25 volumes of chloroform followed by centrifugation for 3 min at 20,000 g. The upper phase was discarded, the same volume of methanol added and centrifuged for 3 min at 20,000 g. The precipitate was dried and taken up in LDS-sample buffer containing reducing agent (Invitrogen), denatured for 10 min at 95 °C and separated by Bis-Tris denaturing SDS-PAGE.

2.7. Assessment of cell death

Cells were cultured in serum-free RPMI w/o phenolred, with 1% ITS-G, L-glutamine and penicillin/streptomycin and stimulated as indicated. Cells treated with 0.1% TritonX-100 were used as death positive control. LDH-release into supernatant was determined with the Cytotoxicity Detection Kit PLUS (Roche Applied Science, Mannheim, Germany) following manufacturer's instructions.

2.8. Immunofluorescence staining, confocal and fluorescence microscopy

THP-1 cells were incubated on collagen coated culture slides (BioCoat 8-Well Collagen Culture Slide, BD 354630) and differentiated with 2.5 ng/ml PMA overnight, primed and stimulated as indicated and fixed in 4% paraformaldehyde (Sigma-Aldrich, St. Louis, MO) for 15 min at room temperature, washed and permeabilized in PBS containing 0.04% saponin (Sigma-Aldrich, St. Louis, MO) and 1% BSA (Sigma-Aldrich, St. Louis, MO) for 1 h. Next, cells were stained with appropriate primary antibodies for 1 h, followed by staining with fluorochrome-labeled secondary antibodies for 45 min. Cover slips were mounted on glass slides in 4,6-Diamidin-2-phenylindol (DAPI) containing Vectashield mounting medium from Vector Laboratories (Burlingame, CA). Slides were subjected to imaging on an inverted Zeiss LSM 510 confocal microscope (Carl Zeiss, Jena, Germany) with a 40× or 63× 1.4NA objective lens or on an inverted Leica TCS SP5 microscope (Leica Microsystems, Wetzlar, Germany) using a Leica HC PL APO 40×/0.7NA. An argon laser was used for excitation of Alexa Fluor 488 at wavelengths of 488 nm, whereas a helium-neon laser (543 nm) was used for excitation of mCherry, and a Laser Diode (405 nm) for the excitation of Hoechst or DAPI.

2.9. Cell proliferation assay

Cell proliferation was assayed using an IncuCyte® ZOOM Live-Cell Analysis System (Essen BioScience, Ann Arbor, MI, USA), by collecting real-time data of cell confluence. Cells were seeded on 96-well plates (4000 cells/well) and analyzed over 40 h. Cell confluence was monitored and data were obtained by analyzing the cell confluence increment over time using the IncuCyte S2 software and expressed as percentage relative to time point 0. Experiments were conducted with three replicates for each experimental condition, two to four image fields per well and repeated at least three times.

2.10. Phagocytosis assay

Phagocytosis was assayed using an IncuCyte® ZOOM Live-Cell Analysis System (Essen BioScience, Ann Arbor, MI, USA). Cells were seeded on 96-well plates (4000 cells/well), treated with 2.5 ng/ml PMA for 24 h. pHrodo™ Green *E. coli* BioParticles® were added, and the increase of green fluorescence was analyzed by scanning the plate and acquiring fluorescent and phase-contrast images in real time. Two to three images per well from three technical replicates were taken every 20 min for 4 h using a 20× objective lens. Images were analyzed using the IncuCyte® Basic Software and expressed as percentage of green object confluence increase relative to time point 0. Green channel acquisition time was 400 ms. Cell segmentation was achieved by applying a mask in order to exclude cells from background. An area filter was applied to exclude objects below 50 μm^2. Green channel background noise was subtracted with the Top-Hat method of background non-uniformity correction. Fluorescence signal was quantified applying a mask.

2.11. Real-time deformability cytometry (RT-DC)

RT-DC in combination with a custom-made image analysis algorithm allows determination of properties of single cells such as cell size, contour and deformation in real-time.25 In brief, THP-1 cells with a shRNA knockdown of endogenous procaspase-1 and re-constitution of procaspase-1 wildtype or variants were differentiated to macrophages with PMA (2.5 ng/ml) over night and primed with LPS (2 μg/ml) for 3 h. Cells were centrifuged at 300 *g* for 10 min and resuspended in PBS (2×10^6 cells/300 μl) without magnesium and calcium with 0.5% methylcellulose (36718 Methyl cellulose, viscosity 4000 cPs, Alfa Aesar). Cells were stimulated in this solution with 5 μM nigericin directly before measuring. The cell suspension was flowed through a microfluidic channel constriction of 30 μm width at a flow rate of 0.16 μl/s and measured for 45 min every 3 min. Every single cell was illuminated with an LED and imaged with a camera. After background subtraction, the contour is determined in real-time and cells are computed in real-time. Inertia ratio and volume of the cell were also calculated based on the contour, as described in 26. In brief, the inertia ratio origins from the second moment of area, and is the ratio of elongation in flow direction and orthogonal to it. Volume of cells is computed by a mathematical rotation of the contour around the axis defined by the centroid of the cell and the flow direction.26 The algorithms to obtain inertia ratio and volume as well as all other analysis tool for RT-DC data are available through the open source software ShapeOut 0.8.8. (available at https://github.com/ZELLMECHANIK-DRESDEN/ShapeOut).

2.12. Statistics

Statistical analysis was performed using GraphPad Prism and SPSS software. Statistical analysis for IL-1β secretion (out of 7 independent experiments) was examined using two-way Anova and multiple comparison test adjusted by Bonferroni. For LDH assay analyses we used two-way Anova repeated measures by both factors with multiple comparisons against GFP-WT (adjusted by Dunnett). The statistical significance for the cumulative numbers of specks (out of 4 independent experiments) was determined using two-way Anova and multiple comparison test adjusted by Bonferroni. The statistical analysis for speck diameters was performed using one-way Anova with Sidiak's multiple comparison test. *P*-values are indicated by *, $p < 0.05$; **, $p < 0.01$; *** $p < 0.001$, or n.s. = not significant.

3. Results

3.1. Generation of genetically modified human monocyte cell lines expressing variant procaspase-1

To investigate whether *CASP1* variants p.R240Q, p.L265S and p.C285A1 influence proliferation, phagocytosis, and cell death of human monocytes/macrophages, we generated an *in vitro* model of a virally transduced human monocytic cell lines (THP-1). Initially, we induced shRNA-mediated knock-down of endogenous procaspase-1 (THP-1/a-PCasp1, down to ~20%) followed by reconstitution of caspase-1 expression with plasmids either encoding for wild-type (WT) or variant procaspase-1 (p.R240Q, p.L265S and an artificial p.C285A variant with an active center mutation, Fig. 1A-C and Suppl. Fig. 1A-C) linked or not linked to fusion-reporter proteins. Transduction efficiency was tested by flow cytometry (data not shown), Western blotting (Fig. 1A,B and Suppl. Fig. 1A-C) and quantitative RT-PCR (Fig. 1D). Despite comparable mRNA expression between cell lines generated, protein expression differed repeatedly between cell lines with higher protein levels in cells reconstituted with the WT fusion reporter when compared to procaspase-1 variants (already reported in1). Of note, comparable protein expression levels were achieved for tagged and untagged cell lines with a multiplicity of infection (MOI) of 0.06 with the exception of the p.L265S variant, which showed repeatedly lower protein expression levels (Fig. 1A). Thus, "untagged" cell lines served as controls for further experiments with the fusion-reporter protein transduced THP-1/a-PCasp1 cells.

To determine cell proliferation, cell health and viability of all cell lines generated, we used the real-time quantitative live cell imaging IncuCyte® platform (Essen Bioscience) and quantified cell confluence over time. As shown in Suppl. Fig. 1D, cell proliferation was not affected by fluorescent tags and did not show differences for the analyzed procaspase-1 variants when compared to wildtype cells.

The biological functionality of the generated THP-1 monocyte model was further evaluated priming cells with LPS, followed by NLRP3-inflammasome stimulation with either nigericin or ATP. IL-1β secretion, measured by cytometric bead array (CBA) (Fig. 1E, Suppl. Fig. 1B) and Western blot analysis of cell culture supernatants (Fig. 1F, Suppl. Fig. 1B), was used as readout for caspase-1 activation. In response to priming with ultrapure LPS (uLPS) and stimulation with nigericin, cells expressing WT procaspase-1 (GFP-WT, WT) secreted significantly more mature IL-1β as compared to GFP control cells or the inactive procaspase-1 variants p.C285A (Fig. 1E, Suppl. Fig. 1B) and p.L265S (Suppl. Fig. 1B). Consistent with these observations, we were able to detect mature IL-1β by Western blotting in the supernatant of cell lines challenged under the same conditions (Fig. 1F, Suppl. Fig. 1B). There are clear differences in mature IL-1β release between WT and p.L265S or p.R240Q after stimulation with ultrapure LPS (uLPS) + nigericin. Using crudeLPS (cLPS), which contains other bacterial components (beside LPS) and therefore activates other TLRs, subsequently inducing the transcriptional regulator NF-κB resulting in caspase-1-dependent and/or independent pro-inflammatory cytokine expression, we see almost no differences after stimulation with nigericin (Fig. 1F).

3.2. Procaspase-1 variants influence pyroptosome formation

A characteristic sign of inflammasome activation within cells is the formation of a perinuclear ASC speck, which can also be referred to as pyroptosome5,8 or even as inflammasome,11 containing multimerized sensor (*e.g.* NLRP3), adaptor (ASC), and effector (caspase-1) proteins. In murine cells we previously demonstrated that procaspase-1 and the enzymatically inactive p.C284A variant are recruited to the pyroptosome.27 Therefore, we performed experiments to determine whether human monocyte cell lines bearing procaspase-1 variants p.R240Q, p.L265S and p.C285A exhibit speck formation in response to inflammasome activation, and if speck formation differs between variants.

Presuming that the monocyte cell model generated sufficiently reproduces physiological macrophage functions *in vitro* and is not affected by fluorescent tags (see Fig. 1 and Suppl. Fig. 1), we conducted live cell imaging experiments with THP-1/a-PCasp1 cells reconstituted with either WT or variant procaspase-1 fusion-reporter proteins. THP-1 monocytes were differentiated to macrophages overnight using 2.5 ng/ml phorbol 12-myristate 13-acetate (PMA). In response to stimulation with LPS alone, cells did not show remarkable changes (data not shown). After priming with LPS followed by the addition of nigericin, GFP-WT and variant procaspase-1 cell lines (GFP-C285A, GFP-L265S, and GFP-R240Q) formed one cytosolic macromolecular speck after approximately 45–60 min, which remained visible for > 5 h (Fig. 2A,B). Consistent with previous observations,27 the p.C285A variant resulted in bigger and significantly brighter speck formation when compared to WT cells. Remarkably, procaspase-1 variant p.L265S resulted in significantly decreased speck numbers and reduced signal intensity. Speck number and intensity in the p.R240Q variant were comparable to those in WT, but showed increased speck size.

Next, we tested whether GFP-WT or GFP-L265S specks had resolved before detection by microscopy contributing to the differences observed regarding speck numbers at time point 310 min (Fig. 2A). To achieve this, we analyzed speck numbers on images acquired from a time-series (over 6 h after NLRP3 stimulation with nigericin at 10 min intervals). The number of newly formed specks were added to speck number on previous slides at each time point, gaining a cumulative speck number (Fig. 2B,C). Differences described above (Fig. 2A) were confirmed with significantly decreased numbers of specks/pyroptosomes in procaspase-1 variants p.C285A and p.L265S when compared to WT and p.R240Q at the time points 240, 300 and 360 min.

Interestingly, speck sizes did not associate with enzyme activity of procaspase-1 variants. To quantify speck sizes, we used the "mean of half maximum intensity" method and analyzed the fluorescence microscopy images, which have been acquired for the experiments in Fig. 2A-C and determined a mean procaspase-1 speck diameter of 1.21 μm (SD ± 0.336) in GFP-WT cells, 1.44 μm (SD ± 0.496) in GFP-C285A cells, 1.12 μm (SD ± 0.361) in GFP-L265S cells and 1.44 μm (SD ± 0.517) in GFP-R240Q cells. Specks of GFP-C285A and GFP-R240Q cells were significantly larger when compared to GFP-WT specks. Specks in GFP-L265S cells were smaller when compared to those in GFP-WT cells, which, however, did not reach statistical significance ($p = 0.07$) (Fig. 2D). Therefore, we performed higher resolution imaging using a confocal microscope. Using this more precise tool, as shown in Fig. 2E, specks for the procaspase-1 p.L265S variant were determined significantly smaller when compared to WT specks.

Using life cell fluorescence microscopy imaging, we noticed differences in speck intensities between cell lines (Fig. 2A). Measuring speck intensities over time, we observed procaspase-1 specks fading in GFP-WT cells almost immediately after their formation (within 20 min) (Fig. 2F). GFP-R240Q specks remained slightly brighter and fading occurred slower (within 40 min), and signal intensities remained at a

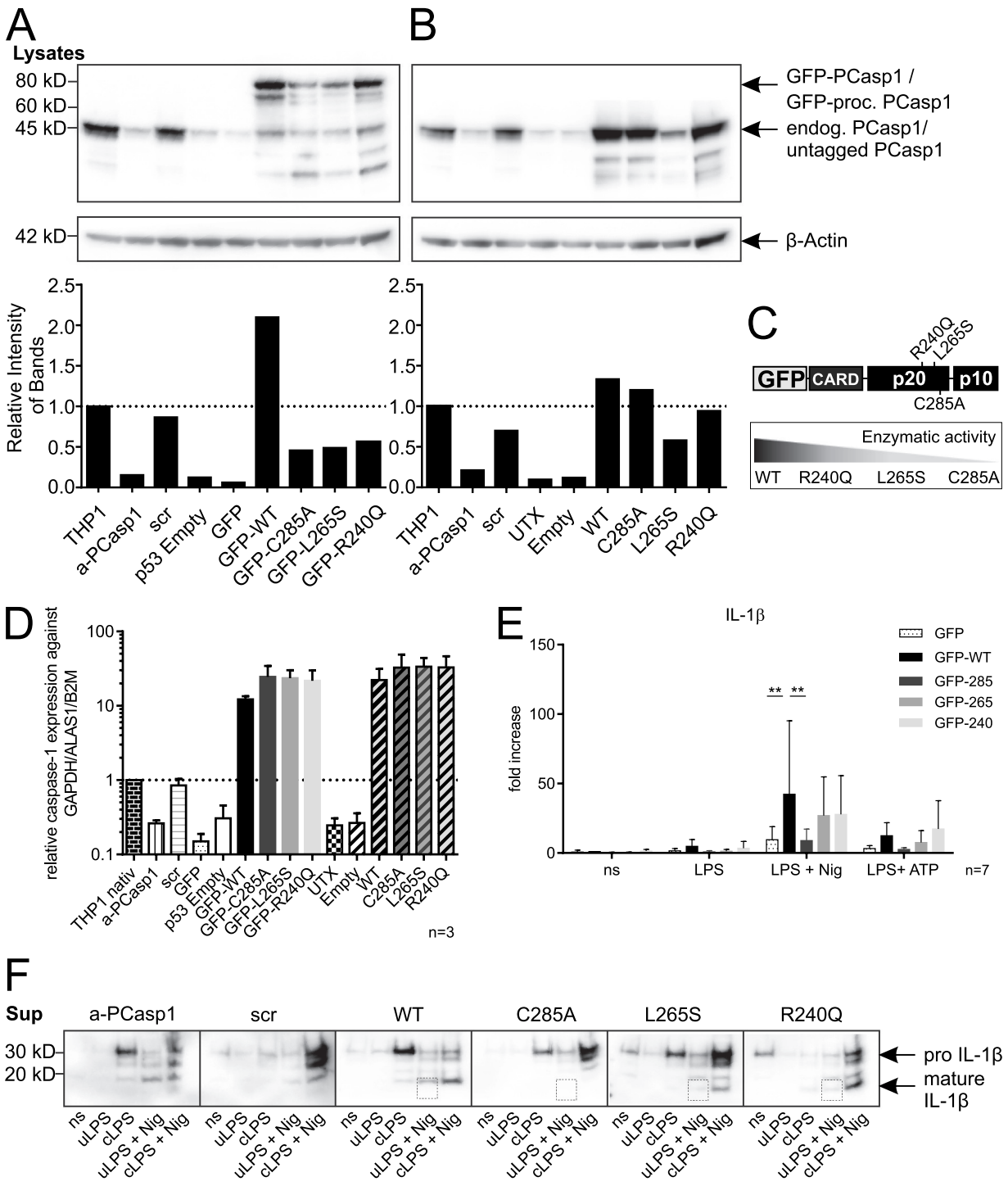

Fig. 1. Generation of human monocytic cell lines with procaspase-1 knock-down and expression of fluorophore-tagged procaspase-1 variants. Fusion proteins of the green fluorophore (EGFP) tagged to either wildtype procaspase-1 (WT) or enzymatic inactive (p.C285A) or attenuated (p.L265S, p.R240Q) procaspase-1 variants were expressed in THP-1 cells carrying a knock-down of the endogenous procaspase-1 (a-PCasp1). Caspase-1 activation was induced by priming with 1 μg/ml ultrapure LPS (uLPS) for 3 h, followed by 10 μM nigericin or 2 mM ATP for 1 h. A,B Western blot analysis shows a highly efficient knock-down of endogenous procaspase-1 (a-PCasp1) with a reduction of protein levels down to ~20%. Protein level (CARD-detecting antibody) of procaspase-1 fusion protein (GFP-PCasp1, 74 kDa), partially degraded caspase-1 (60 kDa) and endogenous or untagged procaspase-1 (~50 kDa) are shown. Quantification (densitometric analysis of Western blots) of caspase-1 expression compared to β-Actin (loading control). C, Schematic drawing of procaspase-1 WT and variants. The fluorescent protein (EGFP) was fused to the N-terminal CARD of procaspase-1. The analyzed mutations localize to the p20 subunit of procaspase-1. D, Caspase-1 expression of a-PCasp1 cell lines reconstituted with WT or variant procaspase-1 measured by qRT-PCR. The relative mRNA expression was calculated as fold-increase compared to three reference genes (*GAPDH/ALAS1/B2M*). E + F, IL-1β release into supernatants was measured by cytometric bead array (E) and Western blot analysis (F). GFP-WT cells secreted significantly more mature IL-1β compared to the inactive procaspase-1 variant p.C285A and GFP-control when treated with both uLPS and nigericin. IL-1β is displayed as fold increase compared to unstimulated GFP-WT cells. A,F, Data are representative of three independent experiments. D,E, Experiments are displayed as the mean ± SD. ns, not stimulated; WT, wildtype; scr, scramble shRNA; empty, reconstitution performed with empty vector; Sup, supernatant; cLPS, crude LPS; ** $p < 0.01$.

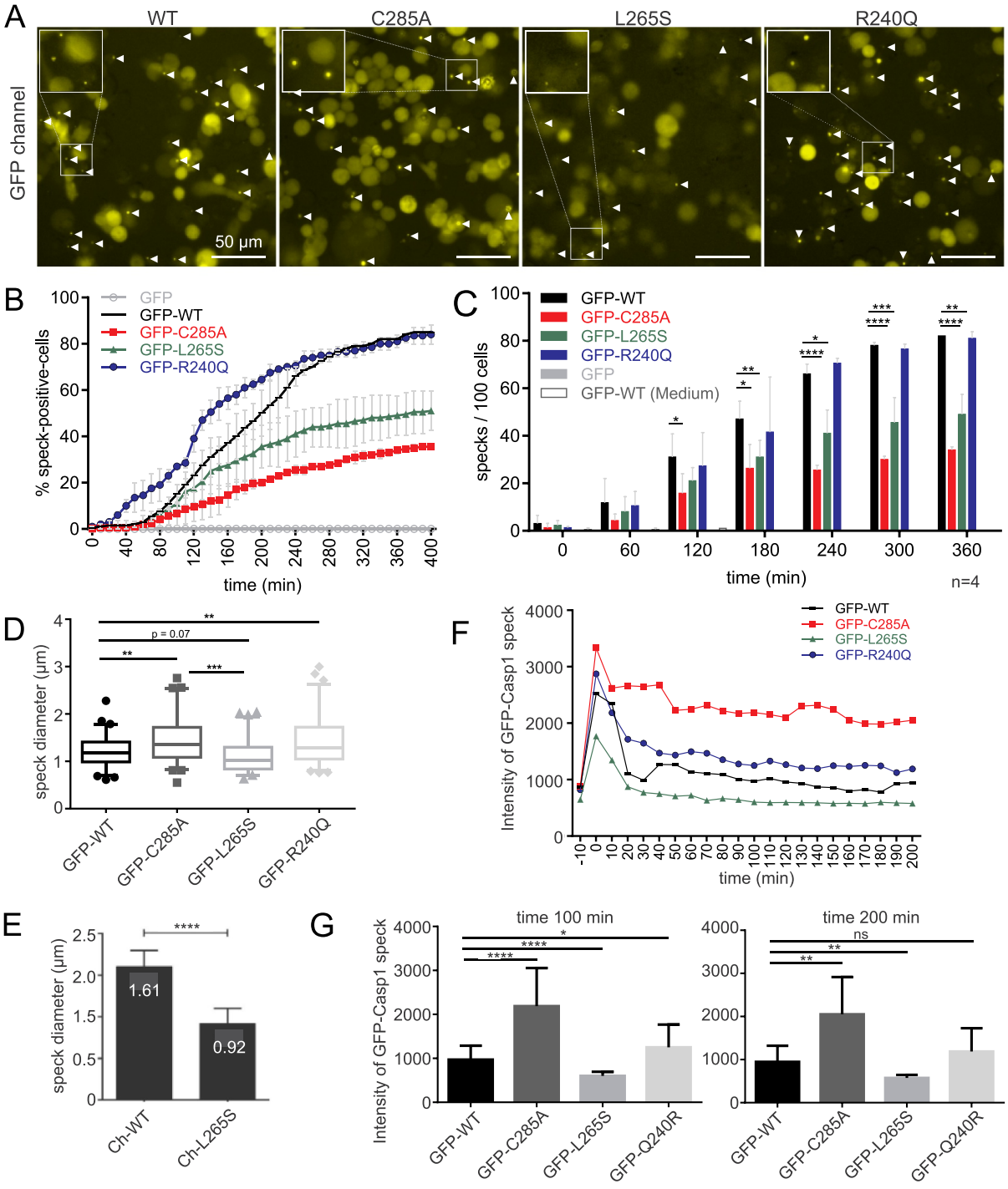

Fig. 2. Enzymatically attenuated procaspase-1 variants affect pyroptosome number, size and intensity. Fusion proteins of EGFP tagged to either WT or enzymatic inactive or attenuated (p.C285A, p.L265S, p.R240Q) procaspase-1 variants were expressed in THP-1 cells with knock-down of the endogenous procaspase-1 (a-PCasp1). Cells were differentiated with 2.5 ng/ml PMA to macrophages overnight. Caspase-1 activation was induced by priming with 1 µg/ml LPS for 3 h, followed by 10 µM nigericin and analyzed by life-cell imaging. A, Representative fluorescence microscopy images of GFP-procaspase-1 specks at time point 310 min after the addition of nigericin are shown. Arrowheads indicate formed specks. B, Life-time images of the fluorescence channel were aquired every 10 min over a time period of 400 min. At each time point, specks emerging for the first time were counted and added to the number of specks in previous slides. Specks were counted and related to the total amount of nuclei (DAPI stains) within the same field. Between 700 and 1000 cells per cell line were analyzed for speck formation. Results of two independent experiments are shown, which are representative for a total of 4 independent experiments. C, GFP-procaspase-1 specks, that were observed by fluorescence microscopy after 60, 120, 180, 240, 300 and 360 min (B) were counted and related to the total amount of nuclei (DAPI stains). Cumulative numbers of specks out of 4 independent experiments are shown. Statistical significance was determined using two-way Anova and multiple comparison test adjusted by Bonferroni. D, Speck size/diameter in cells expressing GFP-WT or GFP-tagged procaspase-1 variants was measured from fluorescence microscopy images (n = 70 specks/cell line out of 4 independent experiments; one-way Anova with Sidiak's multiple comparison test). E, Speck size in cells expressing Ch-WT or Ch-tagged procaspase-1 variant p.L265S was measured from confocal images (n = 20 specks/cell line out of 5 independent experiments; unpaired t-test, mean ± SD). F, As demonstrated in A, specks of the procaspase-1 variant cell lines show differences in their intensity. Graphs indicate mean values of maximum fluorescence intensities of GFP-WT or GFP-tagged procaspase-1 variant specks. First speck formation was set as the starting point (0 min) and assessed for each pyroptosome individually. Intensity levels 10 min before speck formation (−10 min) represent the background signal from the cytosol. Speck intensities after 100 and 200 min were chosen for statistical analysis in G (n = 22/each time point). (For interpretation of the references to colour in this figure legend, the reader is referred to the web version of this article).

higher level when compared to GFP-WT. Specks in GFP-L265S cells only reached a signal intensity that was around 2/3 of that in GFP-WT cells, which faded within 20 min (almost to the background before pyroptosome formation) (Fig. 2F, −10 min time point). In contrast, GFP-C285A specks remained more stable and showed significantly slower fading. Differences were quantified at time points 100 min and 200 min (Fig. 2G) demonstrating significantly brighter specks in GFP-C285A and significantly dimmer specks in GFP-L265S when compared to GFP-WT cells.

As demonstrated previously,27 within the same cell, WT caspase-1 specks decrease more rapidly in fluorescence intensity when compared to ASC stained specks, suggesting caspase-1 auto-processing as a possible explanation. Here, we also demonstrate rapid speck fading and decreased speck intensity in cells expressing variant procaspase-1 p.L265S, which lacks enzymatic activity.1 Assuming that p.L265S is not capable of auto-processing, we wondered about dynamics and distribution of caspase-1 subunits. Thus, we stained stimulated THP-1/a-PCasp1 cells reconstituted with either mCherry (Ch) or the fluorescent fusion proteins Ch-WT or Ch-L265S (all with comparable protein expression, Suppl. Fig. 1C) with antibodies directed against CARD, the p10 or p20 subunit of caspase-1 (Fig. 3A). Both in Ch-WT and Ch-L265S cells, specks co-localized with CARD, p10 and p20. We concluded that mCherry signals represent the localization of procaspase-1 within speck, as has been previously demonstrated by our group for the murine p.C284A variant.27 Furthermore, in Ch-WT and Ch-L265S cells, procaspase-1 specks co-localize with ASC after NLRP3 stimulation (Fig. 3A). In contrast to reduced numbers of caspase-1 specks in Ch-L265S cells when compared to Ch-WT macrophages, all cell lines (Ch-WT, Ch-L265S, Ch) generated the same amount of ASC-specks (Fig. 3B).

Furthermore, in both cell lines, Ch-WT and Ch-L265S, nigericin stimulation resulted not only in speck formation but also in pyroptosis, shown by an increase in cell volume, the presence of cell membrane vesicles, and a decrease in intracellular mCherry fluorescence intensity due to the release of plasma membrane vesicles (Suppl. Fig. 1E + Suppl. Fig. 2A).

3.3. Variant procaspase-1 p.L265S exhibits disturbed subcellular localization

To study subcellular localization of procaspase-1 in macrophages, we performed life cell confocal laser scanning microscopy of PMA-differentiated THP-1 macrophages, showing cytoplasmic and nuclear localization of the mCherry signal in WT cells (Fig. 3C,D). Interestingly, Ch-WT cells, in which functional caspase-1 can self-process, exhibited predominantly nuclear localization of the CARD domain and the p10 subunit, but not of the p20 subunit. Cells with the enzymatically attenuated procaspase-1 variant p.L265S (Ch-L265S) almost exclusively exhibited caspase-1 localization to the cytoplasm (Fig. 3C,D).

To exclude the possibility that subcellular distribution of fusion reporter proteins differs from endogenous procaspase-1 localization, we performed antibody staining of endogenous procaspase-1 using native THP-1 cells (Suppl. Fig. 2B). Corresponding to results in Ch-WT cells, we observed slightly increased fluorescent signal for CARD in the nucleus. In contrast, p20 and p10 subunits distributed almost equally between the nucleus and the cytoplasm.

Since antibody staining against the procaspase-1 subunits did not allow to distinguish between the endogenous and transduced fluorescent reporter fusion protein, we performed experiments in HEK293T cells, which lack endogenous procaspase-1 and pro-IL-1β. We transfected HEK293T cells with Ch, Ch-WT and Ch-L265S together with pro-IL-1β expression plasmids. Western blot analysis showed comparable protein expression, and CBA assays the expected IL-1β secretion in Ch-WT but not in Ch-L265S cells (data not shown). Using confocal laser scanning microscopy, we detected primarily cytoplasmic localization of the p.L265S variant, which was also shown by antibody staining of the caspase-1 subunits CARD, p20 and p10 (Suppl. Fig. 2C).

Taken together, these results demonstrate that the fluorescent reporter attached to CARD does not influence subcellular distribution of procaspase-1 variants. Macrophages with variant procaspase-1 p.L265S, however, exhibit disturbed nuclear localization of caspase-1 when compared to cells expressing wild-type caspase-1 or the other procaspase-1 variants (p.C285A, p.R240Q).

3.4. Procaspase-1 variants do not influence phagocytic capacity of macrophages

One major function of monocytes and macrophages is phagocytosis. To address the question of whether procaspase-1 variants influence phagocytosis, we used the real-time quantitative live cell imaging IncuCyte® platform (Essen BioScience) and analyzed the different cell lines for the capacity to phagocytose pHrodo® Green *E. coli* BioParticles®. Of note, phagocytosis between the cell lines did not vary significantly (Fig. 4).

3.5. Procaspase-1 variants influence gasdermin D processing and pyroptosis

Knowing that procaspase-1 variants influence speck formation and IL-1β maturation and therefore the canonical inflammasome pathway, we investigated their influence on gasdermin-mediated programmed cell death, pyoptosis. Gasdermin D (GSDMD) is a substrate of caspase-1 and caspase-11/4/5. It induces pore formation in the plasma membrane of monocytes/macrophages through its N-terminal fragment, which oligomerizes and inserts in the plasma membrane giving rise to rapid cell lysis. The C-terminal part of GSDMD has inhibitory function and protects from pyroptosis.4,28 THP-1/a-PCasp1 cells either bearing WT procaspase-1 or variants were differentiated to macrophages using PMA, followed by priming with LPS and stimulation with nigericin to induce inflammasome assembly. Activation of WT procaspase-1 through the canonical inflammasome pathway led to GSDMD cleavage and the release of its N-terminal fragment, whereas enzymatically attenuated procaspase-1 variants showed abrogated (p.C285A) or decreased (p.L265S, p.R240Q) GSDMD cleavage (Fig. 5A).

Furthermore, after priming with LPS, the addition of nigericin resulted in a significant increase of lactate dehydrogenase (LDH) release into supernatants of WT transduced cells, which was used as a measure of non-apoptotic inflammatory cell death (Fig. 5B). Procaspase-1 variants also showed an increased LDH release after nigericin stimulation, which, however, was lower when compared to WT cells.

3.6. Procaspase-1 variants influence deformability of macrophages after inflammasome stimulation

Since migration of macrophages into tissues requires activation and cell deformation, we tested whether procaspase-1 variants influence morphological properties of cells.29 THP-1/a-PCasp1 cells bearing WT or variant procaspase-1 were differentiated to macrophages using PMA, primed with LPS and stimulated with nigericin. Using the recently developed technique of real time deformability cytometry (RT-DC), macrophages were deformed in a microfluidic channel constriction of 30 μm, and mechanical and morphological cell parameters were measured in real-time.25,30 The inertia ratio, a parameter that quantifies deformation, and cell volumes were determined at 0 min and 20 min of treatment with nigericin. The measured cell volume was not significantly different between WT (GFP-WT) and procaspase-1 variant cell lines (GFP-240, GFP-265, GFP-285) (Fig. 6A). The inertia ratio, as a measure of deformation, was significantly different at 0 min comparing GFP-WT *versus* GFP-L265S ($p = 0.04764$) cells. 20 min after nigericin stimulation the inertia ratio showed significant differences between GFP-WT and GFP-L265S ($p = 0.04827$) and also between GFP-WT and GFP-C285A ($p = 0.0119$) indicating a higher deformation of the procaspase-1 variants compared to WT (Fig. 6A-C).

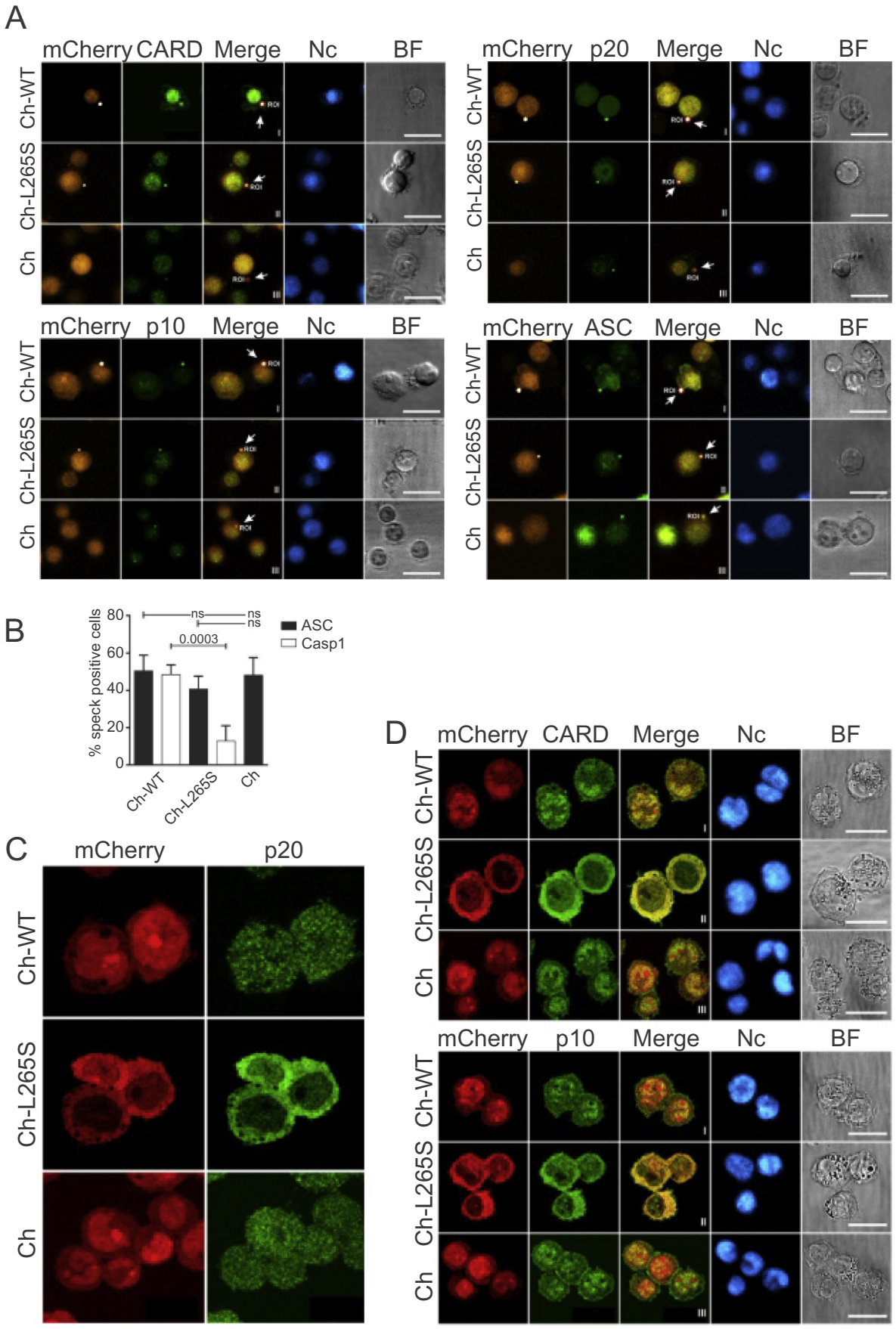

(caption on next page)

Fig. 3. Variant procaspase-1 p.L265S affects pyroptosome size. A, Representative fluorescence microscopy images of THP-1 cells with knock-down of the endogenous procaspase-1 (a-PCasp1) reconstituted with mCherry (Ch)-WT or Ch-L265S (red channel). Cells were differentiated with 2.5 ng/ml PMA to macrophages overnight. Caspase-1 activation was induced by priming with 1 μg/ml LPS for 3 h, followed by 20 μM nigericin for 1 h. Antibody staining against ASC or the CARD, p20 or p10 subunit of caspase-1 (green channel). The overlay of the red and green channel is shown as "Merge". Nuclei were stained with DAPI (blue channel). Ch-WT and Ch-L265S co-localized with CARD, p10 and p20 in all pyroptosomes (Merge), whereas Ch control cells did not show pyroptosome formation in the red channel, however, some pyroptosomes in the green channel (antibody staining), corresponding to the residual endogenous procaspase-1 after shRNA knockdown or to endogenous ASC. B, Quantification of speck positive cells compared to the total cell number of the image (n = 700 cells/cell line out of 4 independent experiments; mean ± SD). Interestingly, in contrast to diminished numbers of Ch-L265S specks compared to Ch-WT, all cell lines (Ch-WT, Ch-L265S, Ch) generated the same amount of the ASC-specks. C + D, Macrophages with variant procaspase-1 p.L265S showed disturbed nuclear localization compared to WT. Representative confocal microscopy images of THP-1 cells with knock-down of the endogenous procaspase-1 (a-PCasp1) reconstituted with Ch, Ch-WT or Ch-L265S (red channel). Cells were stained with antibodies targeting the CARD, p20 or p10 subunit of caspase-1 (green channel). The enzymatically attenuated procaspase-1 variant p.L265S (Ch-L265S) almost exclusively localized to the cytoplasm when fused to mCherry at their N-terminus. (For interpretation of the references to colour in this figure legend, the reader is referred to the web version of this article.)

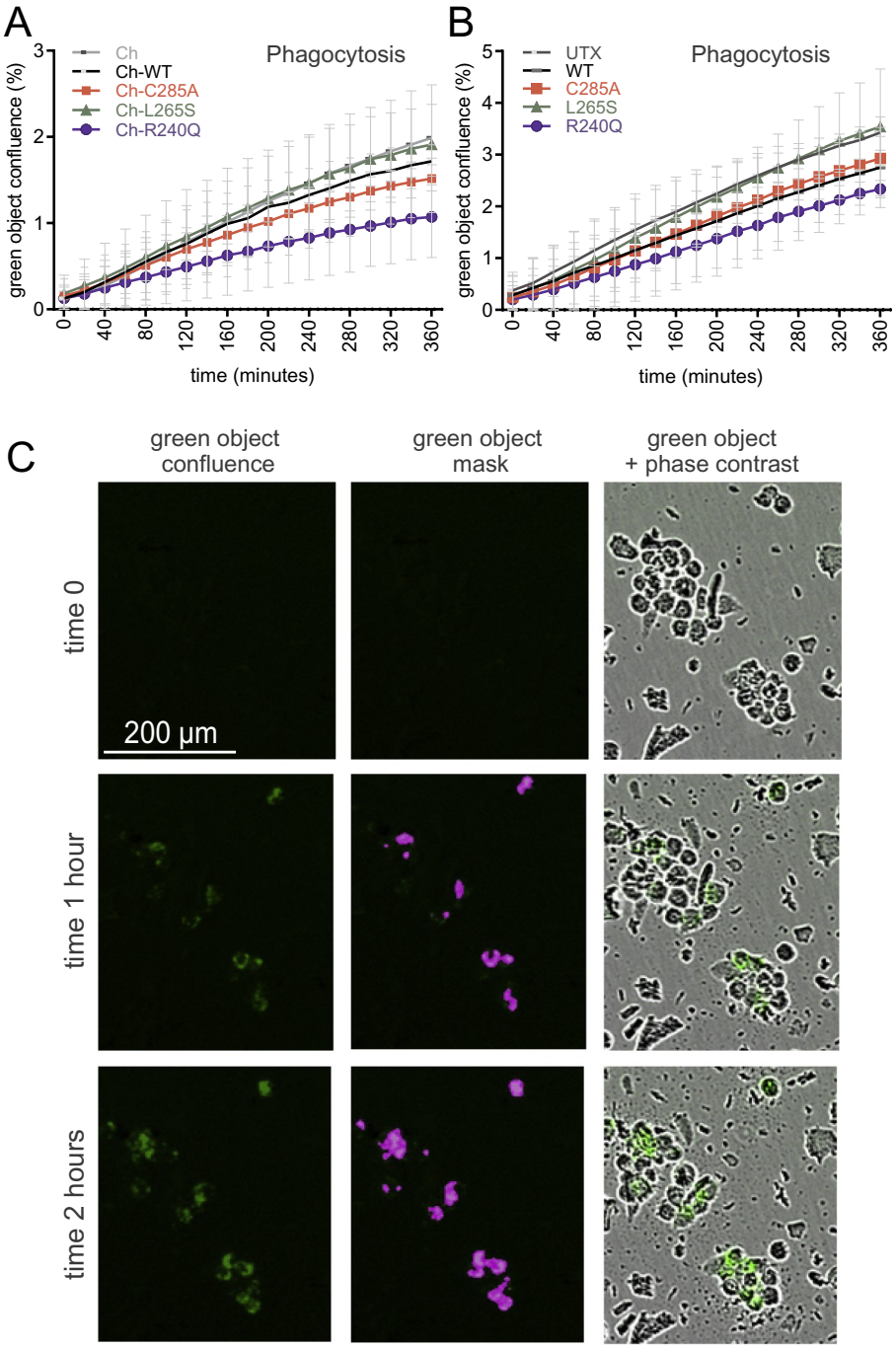

Fig. 4. Procaspase-1 variants do not influence phagocytosis of THP1 macrophages. A + B, THP-1 cells with knock-down of the endogenous procaspase-1 (a-PCasp1) reconstituted with WT and procaspase-1 variants (A, mCherry fusion proteins or B, "untagged") were differentiated with 2.5 ng/ml PMA to macrophages overnight. Analysis of phagocytic capacity of cell lines to phagocytose pHrodo® Green *E. coli* BioParticles®, which only fluoresce when localized in the acidic environment of phagolysosomes (IncuCyte®). Aquired images were quantified for green object confluence (%) for each time point over 4 h. C, Representative images of fluorescence object quantification are shown at time point 0, 1 and 2 h. (For interpretation of the references to colour in this figure legend, the reader is referred to the web version of this article.)

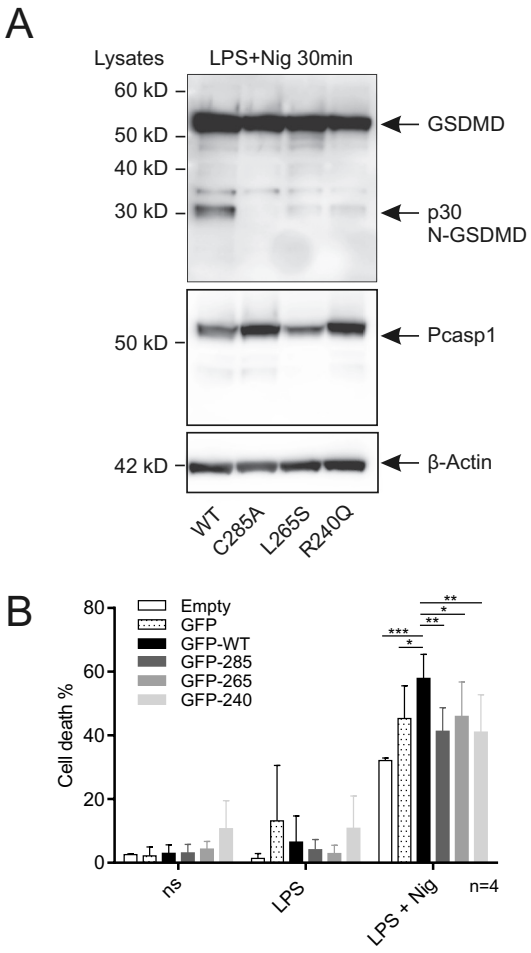

Fig. 5. Procaspase-1 variants influence gasdermin D processing and pyroptosis. A, THP-1/a-PCasp1 cells bearing procaspase-1 WT or variants were differentiated to macrophages with PMA, LPS-primed and stimulated with nigericin. The activation of WT procaspase-1 led to GSDMD cleavage and the release of its N-terminal fragment (p30), whereas enzymatically attenuated procaspase-1 variants show abrogated (p.C285A) or decreased (p.L265S, p.R240Q) GSDMD cleavage. A representative Western blot analysis is displayed. B, After LPS priming the addition of nigericin resulted in a significant increase of lactate dehydrogenase (LDH) release into supernatants of WT transduced cells, representing cell death (n = 4 independent experiments). Procaspase-1 variants also showed an increased LDH release after nigericin stimulation, which was however less compared to WT (two way Anova repeated measures by both factors with multiple comparisons against GFP-WT, Dunnett adjusted).

4. Discussion

We recently showed that *CASP1* variants1,31 that cause an autoinflammatory disease (CASP1-AID) exhibit increased interaction with RIP2, thereby leading to enhanced activation of the pro-inflammatory transcription factor NF-κB. This, in turn may contribute to uncontrolled engagement of inflammatory signaling pathways.3 Since *CASP1* mutations can also occur in asymptomatic family members and rarely in unrelated healthy individuals, questions remain. In this study, we focused on the effects of two disease-associated *CASP1* variants (p.L265S, p.R240Q) and a described missense mutation in the active center of procaspase-1 (p.C285A) on inflammasome/pyroptosome formation, cell proliferation, phagocytic function and mechanical properties of macrophages.

In the past, ASC speck formation was considered essential for IL-1β activation and release but not for pyroptosis.12 Recently, we linked pathologically reduced (pro)caspase-1 activity with increased pyroptosome/speck formation in murine cells.27 Reduced or absent enzymatic activity stabilized the pyroptosome in murine macrophages and resulted in increased speck sizes, intensity and prolonged speck persistence, thus promoting interactions between ASC and procaspase-1 molecules in the pyroptosome. This was independent of the vital state of cells and could occur in the extracellular space after cell lysis. Furthermore, we suggested that pro-inflammatory signal transmission through spreading of specks during cell division may be an additional mechanism amplifying inflammation.27

In the here described system of THP-1/a-PCasp1 cells, reconstitution with either WT or variant procaspase-1, priming with LPS and stimulation of NLRP3 inflammasome assembly with nigericin or ATP resulted in IL-1β release that was proportional to the residual enzymatic activity of procaspase-1 variants. The formation of perinuclear specks/pyroptosomes was differentially influenced by individual procaspase-1 variants regarding number, size and fluorescence intensity of specks and did not correlate with the residual enzymatic activity. Variants p.C285A (an artificial active center mutation) and p.R240Q (occurring as hetero- and homozygous mutation in patients) were associated with increased pyroptosome size and fluorescence intensity, which was comparable to previous findings in the murine p.C284A variant.27 Despite the increased pyroptosome size, these procaspase-1 variants did neither lead to enhanced GSDMD processing nor to increased cell death.

In contrast, the p.L265S procaspase-1 variant (heterozygous mutation in patients) associated with significantly reduced pyroptosome formation when compared to WT caspase-1, smaller procaspase-1 specks and reduced fluorescence, while the size of the ASC specks did not differ. Assuming that the p.L265S variant is not subject to autoprocessing,1 we detected all procaspase-1 subunits inside the specks by antibody staining for CARD, p20 and p10. Confirming our previous data from the murine system,27 we detected all three procaspase-1 subunits inside the WT specks, co-localizing with ASC. Reduced speck formation in cells carrying the p.L265S variant may be explained by protein misfolding.1 This, in combination with the absence of enzymatic activity in this variant (lack of auto-processing), may also contribute to disturbed subcellular localization (“nuclear exclusion”).

Observed differences in speck formation, which do not associate with residual enzymatic activity of tested procaspase-1 variants, suggest that further mechanisms exist that contribute to the pro-inflammatory phenotype in CASP1-AID patients. Thus, usually heterozygous *CASP1* variants may represent a disease modifying factor in the context of other mechanisms that contribute to the expression of CASP1-AID. Since, rarely, healthy individuals carry mutations investigated here, individual factors protecting from disease expression may be present. Currently, it can only be hypothesized whether these include genetic variants (cytokine promoter polymorphisms, HLA variants, *etc.*) or environmental factors (*e.g.* epigenetically determined), protecting from systemic inflammation.

One of the major biological functions of monocytes and macrophages is their capacity as phagocytes. Thus, we analyzed the phagocytic ability of mutant p.R240Q, p.L265S and p.C285A *CASP1* cell lines in response to PAMPs. The capacity to phagocytose pHrodo® Green *E. coli* BioParticles was not different between WT and the analyzed procaspase-1 variants.

Since cytomechanical properties of cells correlate very closely with physiological and pathological changes in cell function, the measurement of cell mechanics as a biophysical characterization method of cytoskeletal changes has been established in recent years.32 The relatively new method of real-time deformability cytometry (RT-DC) allows the characterization of cell alterations associated with remodeling processes. It has been shown that efficient reorganization of the actin cytoskeleton is required for rapid ASC speck formation.33,34 Therefore, impaired speck formation by *CASP1* variants should lead to changes in cytoskeleton compliance. Using RT-DC we analyzed the influence of procaspase-1 variants on cell mechanics and found that *CASP1* variants associate with higher cell deformability. As macrophage migration to

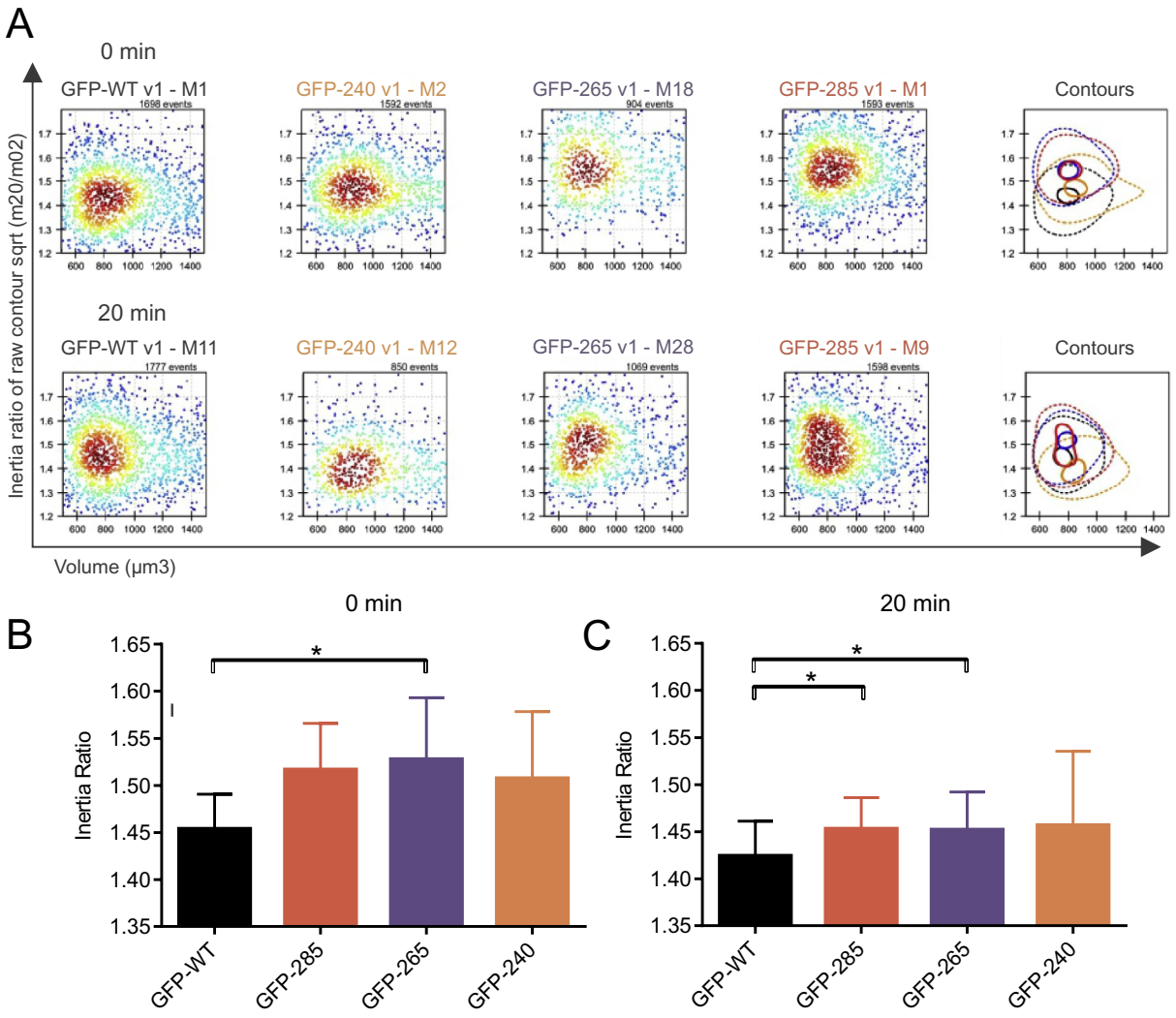

Fig. 6. Morphological and mechanical properties of macrophages. Representative scatter and contour plots (A) and statistical analysis (B) of inertia ratio, indicating increased inertia ratio of GFP-285 and GFP-265 compared to GFP-WT. THP-1 cells were differentiated to macrophages with PMA (2.5 ng/ml), LPS-primed (1 µg/ml, 3 h) and stimulated with nigericin. The inertia ratio as well as the volume (cell size) was determined for measurements taken at 0 min and 20 min of treatment. The cell volume was not significantly different for any of the states (GFP-WT, GFP-240, GFP-265, GFP-285) at any time point. The inertia ratio (I) is a parameter that quantifies deformation ($I = 1$ means circle, higher I means more deformed). Linear mixed models analysis was performed to obtain statistical significance. Analyses have been performed using ShapeOut 0.8.8, *, $p < 0.05$. (For interpretation of the references to colour in this figure legend, the reader is referred to the web version of this article)

tissues requires activation and mechanical deformation, one could speculate that a higher deformation of cells bearing procaspase-1 variants could facilitate the migration of macrophages. In contrast to our results, Ekpenyong et al. reported increased cell rigidity of murine macrophages (BMDM) associated with *S. typhimurium* infection and therefore inflammation.[32] The diverse results could be due to the use of different cell lines (human monocytic cells, THP-1 *versus* BMDM), stimulations (LPS and nigericin *versus S. typhimurium* infection) and techniques (RT-DC *versus* digital holographic microscopy, DHM). Further projects following this hypothesis are warranted and will analyze the exact influences of procaspase-1 variants on cell deformability and migration.

5. Conclusions

Procaspase-1 variants contribute to the inflammatory phenotype in patients with CASP1-AID despite decreased IL-1β processing. In addition to previously reported increased interactions between procaspase-1 variants and RIP2[3] and stabilization of ASC-pyroptosomes,[27] enzymatically attenuated human procaspase-1 variants do not prevent macrophages from pyroptosome formation, but influence the number, size and intensity of pyroptosomes independent of the residual enzymatic activity of caspase-1. Furthermore, human procaspase-1 variants do not influence cell proliferation and phagocytic capacity, however, lead to increased macrophage deformability, which could facilitate cell migration into inflamed tissue.

Data from this study provide new insights into the involvement of caspase-1 in monocyte/macrophage biology and effects of reduced enzyme activity. Further investigations are needed to elucidate the exact molecular effects of *CASP1* variants and modifying genetic and/or environmental factors causing CASP1-AID in some but not other individuals affected.

Supplementary data to this article can be found online at https://doi.org/10.1016/j.clim.2019.06.008.

Author contributions

FK, SR-M and FS conducted most of the experiments and analyzed the results. SRu conducted experiments on the IL-1β secretion of cells and constructed vectors for expression of fluorescently labeled proteins.

MH performed the RT-DC data analysis. CMH, SW, JG, RS and ARW helped with interpretation of data and revised the manuscript. SRH designed the study, conducted some of the *in vivo* live cell imaging experiments and the IncuCyte® experiments, analyzed data and wrote the paper. All authors reviewed the results and approved the final version of the manuscript.

Acknowledgments

Images were generated at the Biopolis Dresden Imaging Platform (BioDIP) including the Biotechnology Center of the TU Dresden (BIOTEC), the Center for Regenerative Therapies (CRTD), and the Core Facility Cellular Imaging (CFCI). The authors thank especially Hella Hartmann (BioDIP/BIOTEC), and Silke Tulok and Anja Nobst (CFCI) for excellent support. We thank Prof. Dirk Lindemann (Dresden, Germany) for kindly providing plasmids. The work was supported by the German Research Foundation (DFG-KFO249, HO4510/1-2 to S.R.H., and RO/471-11 to A.R.W. and S.W.), the Else Kröner Fresenius Stiftung (Else-Kröner-Promotionskolleg, EKFS foundation to S.R-M.), and the Roland Ernst Stiftung für Gesundheitswesen (3/17 to S.R.H). CMH's work is supported by the Fritz-Thyssen Foundation (research grant: SLE), Novartis Pharmaceuticals (research grant: psoriasis), LUPUS UK (research grant: SLE), the Hugh Greenwood Legacy Fund (research grant: bronchial inflammation), the Michael Davie Research Foundation (research grant: CNO/CRMO), and the FAIR charity (research grants: bronchial inflammation and SLE).

Conflicts of interests

The authors declare that the research was conducted in the absence of any commercial or financial relationships that could be construed as a potential conflict of interest. CMH received honoraria for advisory board activities and presentations from Novartis pharmaceuticals and Roche (systemic autoinflammatory disease).

References

[1] H. Luksch, M.J. Romanowski, O. Chara, V. Tüngler, E.R. Caffarena, M.C. Heymann, P. Lohse, I. Aksentijevich, E.F. Remmers, S. Flecks, N. Quoos, J. Gramatté, C. Petzold, S.R. Hofmann, S. Winkler, F. Pessler, T. Kallinich, G. Ganser, A. Nimtz-Talaska, U. Baumann, V. Runde, B. Grimbacher, J. Birmelin, M. Gahr, J. Roesler, A. Rösen-Wolff, Naturally occurring genetic variants of human Caspase-1 differ considerably in structure and the ability to activate interleukin-1β, Hum. Mutat. 34 (2013) 122–131.

[2] K.D. Pruitt, T. Tatusova, G.R. Brown, D.R. Maglott, NCBI reference sequences (RefSeq): current status, new features and genome annotation policy, Nucleic Acids Res. 40 (2012) D130–D135.

[3] M.C. Heymann, S. Winkler, H. Luksch, S. Flecks, M. Franke, S. Russ, S. Ozen, E. Yilmaz, C. Klein, T. Kallinich, D. Lindemann, S. Brenner, G. Ganser, J. Roesler, A. Rosen-Wolff, S.R. Hofmann, Human procaspase-1 variants with decreased enzymatic activity are associated with febrile episodes and may contribute to inflammation via RIP2 and NF-kappaB signaling, J. Immunol. 192 (2014) 4379–4385.

[4] J. Shi, Y. Zhao, K. Wang, X. Shi, Y. Wang, H. Huang, Y. Zhuang, T. Cai, F. Wang, F. Shao, Cleavage of GSDMD by inflammatory caspases determines pyroptotic cell death, Nature 526 (7575) (2015) 660–665, https://doi.org/10.1038/nature15514 Epub 2015 Sep 16.

[5] T. Bergsbaken, S.L. Fink, B.T. Cookson, Pyroptosis: host cell death and inflammation, Nat. Rev. Microbiol. 7 (2009) 99–109.

[6] S. Ruhl, K. Shkarina, B. Demarco, R. Heilig, J.C. Santos, P. Broz, ESCRT-dependent membrane repair negatively regulates pyroptosis downstream of GSDMD activation, Science 362 (2018) 956–960.

[7] J. Masumoto, S. Taniguchi, K. Ayukawa, H. Sarvotham, T. Kishino, N. Niikawa, E. Hidaka, T. Katsuyama, T. Higuchi, J. Sagara, ASC, a novel 22-kDa protein, aggregates during apoptosis of human promyelocytic leukemia HL-60 cells, J. Biol. Chem. 274 (1999) 33835–33838.

[8] T. Fernandes-Alnemri, J. Wu, J.-W. Yu, P. Datta, B. Miller, W. Jankowski, S. Rosenberg, J. Zhang, E.S. Alnemri, The pyroptosome: a supramolecular assembly of ASC dimers mediating inflammatory cell death via caspase-1 activation, Cell Death Differ. 14 (2007) 1590–1604.

[9] K. Kersse, M. Lamkanfi, M.J.M. Bertrand, T. Vanden Berghe, P. Vandenabeele, Interaction patches of procaspase-1 caspase recruitment domains (CARDs) are differently involved in procaspase-1 activation and receptor-interacting protein 2 (RIP2)-dependent nuclear factor κB signaling, J. Biol. Chem. 286 (2011) 35874–35882.

[10] A. Lu, V.G. Magupalli, J. Ruan, Q. Yin, M.K. Atianand, M.R. Vos, G.F. Schröder, K.A. Fitzgerald, H. Wu, E.H. Egelman, Unified polymerization mechanism for the assembly of ASC-dependent inflammasomes, Cell 156 (2014) 1193–1206.

[11] P. Broz, V.M. Dixit, Inflammasomes: mechanism of assembly, regulation and signalling, Nat. Rev. Immunol. 16 (7) (2016) 407–420 Epub 2016 Jun 13.

[12] M.S. Dick, L. Sborgi, S. Ruhl, S. Hiller, P. Broz, ASC filament formation serves as a signal amplification mechanism for inflammasomes, Nat. Commun. 7 (2016) 11929.

[13] A. Baroja-Mazo, F. Martín-Sánchez, A.I. Gomez, C.M. Martínez, J. Amores-Iniesta, V. Compan, M. Barberà-Cremades, J. Yagüe, E. Ruiz-Ortiz, J. Antón, S. Buján, I. Couillin, D. Brough, J.I. Arostegui, P. Pelegrín, The NLRP3 inflammasome is released as a particulate danger signal that amplifies the inflammatory response, Nat. Immunol. 15 (2014) 738–748.

[14] B.S. Franklin, L. Bossaller, D.D. Nardo, J.M. Ratter, A. Stutz, G. Engels, C. Brenker, M. Nordhoff, S.R. Mirandola, A. Al-Amoudi, M.S. Mangan, S. Zimmer, B.G. Monks, M. Fricke, R.E. Schmidt, T. Espevik, B. Jones, A.G. Jarnicki, P.M. Hansbro, P. Busto, A. Marshak-Rothstein, S. Hornemann, A. Aguzzi, W. Kastenmüller, E. Latz, The adaptor ASC has extracellular and 'prionoid' activities that propagate inflammation, Nat. Immunol. 15 (2014) 727–737.

[15] A. Sarkar, M. Duncan, J. Hart, E. Hertlein, D.C. Guttridge, M.D. Wewers, ASC directs NF- B activation by regulating receptor interacting Protein-2 (RIP2) Caspase-1 interactions, J. Immunol. 176 (2006) 4979–4986.

[16] S.K. Ippagunta, R.K.S. Malireddi, P.J. Shaw, G.A. Neale, L. Vande Walle, D.R. Green, Y. Fukui, M. Lamkanfi, T.-D. Kanneganti, The inflammasome adaptor ASC regulates the function of adaptive immune cells by controlling Dock2-mediated Rac activation and actin polymerization, Nat. Immunol. 12 (2011) 1010–1016.

[17] B.B. McConnell, P.M. Vertino, Activation of a caspase-9-mediated apoptotic pathway by subcellular redistribution of the novel caspase recruitment domain protein TMS1, Cancer Res. 60 (2000) 6243–6247.

[18] J. Masumoto, T.A. Dowds, P. Schaner, F.F. Chen, Y. Ogura, M. Li, L. Zhu, T. Katsuyama, J. Sagara, S.i. Taniguchi, D.L. Gumucio, G. Núñez, N. Inohara, ASC is an activating adaptor for NF-κB and caspase-8-dependent apoptosis, Biochem. Biophys. Res. Commun. 303 (2003) 69–73.

[19] M. Molmeret, S.D. Zink, L. Han, A. Abu-Zant, R. Asari, D.M. Bitar, Y. Abu Kwaik, Activation of caspase-3 by the dot/Icm virulence system is essential for arrested biogenesis of the legionella-containing phagosome, Cell. Microbiol. 6 (2004) 33–48.

[20] M. Hasegawa, R. Imamura, K. Motani, T. Nishiuchi, N. Matsumoto, T. Kinoshita, T. Suda, Mechanism and repertoire of ASC-mediated gene expression, J. Immunol. 182 (2009) 7655–7662.

[21] D.J. Taxman, E.A. Holley-Guthrie, M.T.-H. Huang, C.B. Moore, D.T. Bergstralh, I.C. Allen, Y. Lei, D. Gris, J.P.-Y. Ting, The NLR adaptor ASC/PYCARD regulates DUSP10, mitogen-activated protein kinase (MAPK), and chemokine induction independent of the inflammasome, J. Biol. Chem. 286 (2011) 19605–19616.

[22] D.A. Amer, G. Kretzschmar, N. Muller, N. Stanke, D. Lindemann, G. Vollmer, Activation of transgenic estrogen receptor-beta by selected phytoestrogens in a stably transduced rat serotonergic cell line, J. Steroid Biochem. Mol. Biol. 120 (2010) 208–217.

[23] M.C. Heymann, S. Rabe, S. Ruß, F. Kapplusch, F. Schulze, R. Stein, S. Winkler, C.M. Hedrich, A. Rösen-Wolff, S.R. Hofmann, Fluorescent tags influence the enzymatic activity and subcellular localization of procaspase-1, Clin. Immunol. (Orlando, Fla.) 160 (2015) 172–179.

[24] J. Schindelin, I. Arganda-Carreras, E. Frise, V. Kaynig, M. Longair, T. Pietzsch, S. Preibisch, C. Rueden, S. Saalfeld, B. Schmid, J.Y. Tinevez, D.J. White, V. Hartenstein, K. Eliceiri, P. Tomancak, A. Cardona, Fiji: an open-source platform for biological-image analysis, Nat. Methods 9 (2012) 676–682.

[25] O. Otto, P. Rosendahl, A. Mietke, S. Golfier, C. Herold, D. Klaue, S. Girardo, S. Pagliara, A. Ekpenyong, A. Jacobi, M. Wobus, N. Topfner, U.F. Keyser, J. Mansfeld, E. Fischer-Friedrich, J. Guck, Real-time deformability cytometry: on-the-fly cell mechanical phenotyping, Nat. Methods 12 (2015) 199–202 (194 p following 202).

[26] M. Herbig, A. Mietke, P. Muller, O. Otto, Statistics for real-time deformability cytometry: clustering, dimensionality reduction, and significance testing, Biomicrofluidics 12 (2018) 042214.

[27] R. Stein, F. Kapplusch, M.C. Heymann, S. Russ, W. Staroske, C.M. Hedrich, A. Rosen-Wolff, S.R. Hofmann, Enzymatically inactive procaspase-1 stabilizes the ASC-pyroptosome and supports pyroptosome spreading during cell division, J. Biol. Chem. 291 (35) (2016) 18419–18429, https://doi.org/10.1074/jbc.M116.718668 Epub 2016 Jul 8..

[28] N. Kayagaki, I.B. Stowe, B.L. Lee, K. O'Rourke, K. Anderson, S. Warming, T. Cuellar, B. Haley, M. Roose-Girma, Q.T. Phung, P.S. Liu, J.R. Lill, H. Li, J. Wu, S. Kummerfeld, J. Zhang, W.P. Lee, S.J. Snipas, G.S. Salvesen, L.X. Morris, L. Fitzgerald, Y. Zhang, E.M. Bertram, C.C. Goodnow, V.M. Dixit, Caspase-11 cleaves gasdermin D for non-canonical inflammasome signalling, Nature 526 (2015) 666–671.

[29] D.M. Mosser, J.P. Edwards, Exploring the full spectrum of macrophage activation, Nat. Rev. Immunol. 8 (2008) 958–969.

[30] O. Otto, P. Rosendahl, S. Golfier, A. Mietke, M. Herbig, A. Jacobi, N. Topfner, C. Herold, D. Klaue, S. Girardo, M. Winzi, E. Fischer-Friedrich, J. Guck, Real-time

deformability cytometry as a label-free indicator of cell function, Conf. Proc. IEEE Eng. Med. Biol. Soc. (2015) (2015) 1861–1864.
[31] H. Luksch, S. Winkler, M.C. Heymann, F. Schulze, S.R. Hofmann, J. Roesler, A. Rosen-Wolff, Current knowledge on procaspase-1 variants with reduced or abrogated enzymatic activity in autoinflammatory disease, Curr. Rheumatol. Rep. 17 (2015) 45.
[32] A.E. Ekpenyong, S.M. Man, S. Achouri, C.E. Bryant, J. Guck, K.J. Chalut, Bacterial infection of macrophages induces decrease in refractive index, J. Biophotonics 6 (2013) 393–397.
[33] S.M. Man, L.J. Hopkins, E. Nugent, S. Cox, I.M. Glück, P. Tourlomousis, J.A. Wright, P. Cicuta, T.P. Monie, C.E. Bryant, Inflammasome activation causes dual recruitment of NLRC4 and NLRP3 to the same macromolecular complex, Proc. Natl. Acad. Sci. U. S. A. 111 (2014) 7403–7408.
[34] S.M. Man, A. Ekpenyong, P. Tourlomousis, S. Achouri, E. Cammarota, K. Hughes, A. Rizzo, G. Ng, J.A. Wright, P. Cicuta, J.R. Guck, C.E. Bryant, Actin polymerization as a key innate immune effector mechanism to control Salmonella infection, Proc. Natl. Acad. Sci. U. S. A. 111 (2014) 17588–17593.